Numerical Modeling of Edge-Localized-Mode Filaments on Divertor Plates Based on Thermoelectric Currents

A. Wingen,[1] T. E. Evans,[2] C. J. Lasnier,[3] and K. H. Spatschek[1]

[1]*Institut für Theoretische Physik, Heinrich-Heine-Universität Düsseldorf, D-40225 Düsseldorf, Germany*

[2]*General Atomics, San Diego, California 92186-5608, USA*

[3]*Lawrence Livermore National Laboratory, Livermore, California 94550, USA*

(Received 10 June 2009; published 26 April 2010)

Edge localized modes (ELMs) are qualitatively and quantitatively modeled in tokamaks using current bursts which have been observed in the scrape-off-layer (SOL) during an ELM crash. During the initial phase of an ELM, a heat pulse causes thermoelectric currents. They first flow in short connection length flux tubes which are initially established by error fields or other nonaxisymmetric magnetic perturbations. The currents change the magnetic field topology in such a way that larger areas of short connection length flux tubes emerge. Then currents predominantly flow in short SOL-like flux tubes and scale with the area of the flux tube assuming a constant current density. Quantitative predictions of flux tube patterns for a given current are in excellent agreement with measurements of the heat load and current flow at the DIII-D target plates during an ELM cycle.

DOI: 10.1103/PhysRevLett.104.175001 PACS numbers: 52.35.Py, 05.45.Pq, 28.52.Av

Edge localized modes (ELMs) [1] are common phenomena in stationary H-mode plasmas. Control and mitigation of high heat loads expelled by ELMs is a key topic for the next generation fusion devices like ITER. So far, the type-I ELMing H mode (where the ELM instability repeats periodically, typically at high frequency, throughout the H-mode phase of the discharge) is the standard operational scenario for ITER [2]. Extrapolating the energy pulse expelled by ELMs to ITER implies that plasma facing wall materials will suffer from fast erosion or melting [3].

Understanding ELM dynamics beyond the initial linear phase is still in its infancy. Peeling-ballooning theory predicts that a type-I ELM cycle is initiated when an edge ideal MHD mode is destabilized as the pedestal pressure gradient exceeds its linear marginal stability limit [4]. The main ELM burst, i.e., the nonlinear evolution, is poorly understood. Questions like scaling with plasma geometry and operating conditions as well as mitigation by resonant magnetic perturbations (RMPs) lack a good theoretical foundation.

Fast, infrared thermography on ASDEX-U has shown [5] nonaxisymmetric energy deposition patterns at the divertor target plates during ELMs. Important information on ELM filaments stems from observations at the MAST tokamak [6]. Experiments on DIII-D have shown that edge stochastization significantly influences ELM dynamics [7] and plasma-wall interaction. Perturbation coils have been installed in tokamaks, like Tore Supra, TEXTOR, DIII-D, and JET, and will be added to ASDEX-U. In DIII-D RMPs suppressed ELMs [8]. Also in JET ELM mitigation with RMPs was recently achieved [9]. Motivated by these results, a flexible set of RMP coils was added to the ITER design [10,11]. Thus, there is an urgent need for a better theoretical understanding of experimental data from existing devices and a subsequent extrapolation for ITER.

The influence of RMPs on the magnetic topology in DIII-D has been analyzed in great detail. Separatrix splitting into stable and unstable manifolds and connection of internal resonant islands to the targets has been reported [12]. Also, the formation of short connection length flux tubes was shown [13]. The latter connect the target plates through the plasma edge within the perturbed separatrix boundary. Within the flux tubes a coherent nonstochastic structure is maintained while being surrounded by stochastic field lines. We shall use these structures as channels for current and thereby as the starting points for the present investigation.

The role of current channels, especially in the scrape-off layer (SOL), during an ELM has been previously emphasized by Takahashi *et al.* [14]. Here, the observed poloidal perturbation magnetic fields are consistent with field-aligned currents flowing just outside the boundary during ELMs. Simultaneously, an ELM model was proposed by Zheng *et al.* [15]. It considers external MHD mode amplification due to coupling with SOL current. The model predicts a sharp onset and fast growth of magnetic perturbations followed by a quick quenching.

Evans *et al.* [16] proposed a scenario in which an initial pulse of heat and particles is the essential trigger for currents and associated magnetic field perturbations. The initial heat pulse during an ELM is conducted towards the target plates through short connection length flux tubes initially established by error fields or other nonaxisymmetric magnetic perturbations. Because of the different arrival times, the heat pulse instantaneously increases the electron temperature T_e on the outer target relative to the inner

 © 2010 The American Physical Society

target plate. Then, a thermoelectric current is driven between the targets, flowing from the outer to the inner target plate [17]. This current may cause a substantial change in the edge topology of the plasma, which could be the cause for the strongly nonlinear behavior of an ELM. In this Letter we further develop this qualitatively oriented idea up to quantitative predictions.

Let us first show in Fig. 1 a connection length simulation of the lower target area poloidal cross section in DIII-D as produced by error fields and active error field correction (the DIII-D I coil [7,8] is used for error field correction here) before an ELM crash.

The color code represents the connection length of the field lines, which is the field line length inside the vessel between the two target plates. The simulation is constrained to match experimental data from shot no. 133908 at 2000 ms. These data are used as examples for a typical ELMing H mode. In the following, this is referred to as the reference case. As can be seen, the magnetic topology is only slightly perturbed by the combined error and I-coil fields. One flux tube appears, which intersects the poloidal cross section several times, as shown by the small blue areas in Fig. 1. This flux tube has a connection length of about 100 m (approximately two poloidal turns). As discussed in Ref. [13], the flux tube is created by the intersection of the stable and unstable separatrix manifolds. In the following, it will be referred to as tube 1. Its area is approximately 2.1 cm^2, which scales as $1/B$ since the toroidal flux ($B_T\, dA$) is preserved due to the symplectic nature of the Hamiltonian system.

The model presented here consists of two steps. It is based on a conceptual ELM model proposed in Ref. [16]. As far as the decisive role of currents is concerned, it is consistent with other existing ELM models like Refs. [6,14,15]. In the first step an initial current of 300 A is assumed flowing through tube 1. This assumption will be verified later. The magnetic field perturbation of this current severely modifies the topology of the plasma edge. Three main new effects appear. First a connection to the upper target plates is established. The former lower single null configuration turns into a double null configuration. The second effect is that a new type of flux tube appears. The new flux tubes are indirect evidence for the additional connection to the upper targets; the latter is not explicitly shown here. Each of the new flux tubes still connect the two lower targets with each other, but their areas are large, e.g., 22.5 cm^2, compared to tube 1. Also, the connection length is only one poloidal turn (about 50 m), which is half the length of tube 1. The area of these tubes formerly belonged to the SOL.

The modified topology is shown in Fig. 2. As can be seen, several new flux tubes appeared: one-poloidal-turn tubes as well as longer ones similar to tube 1 (also tiny $1\frac{1}{2}$ poloidal turn tubes, connecting the lower to the upper targets). The third effect is that a bifurcation is caused by the current perturbation. In the reference case there is only one flux tube with a certain toroidal phase. In the modified topology every flux tube has a counterpart whose phase is shifted by 180° toroidally. The flux tubes can be ordered in pairs while each pair forms a double helical-like structure.

In the second step we assume that a thermoelectric current flows through the newly created much shorter, one-poloidal-turn flux tubes. Field lines within these tubes have a similar structure as field lines in the unperturbed

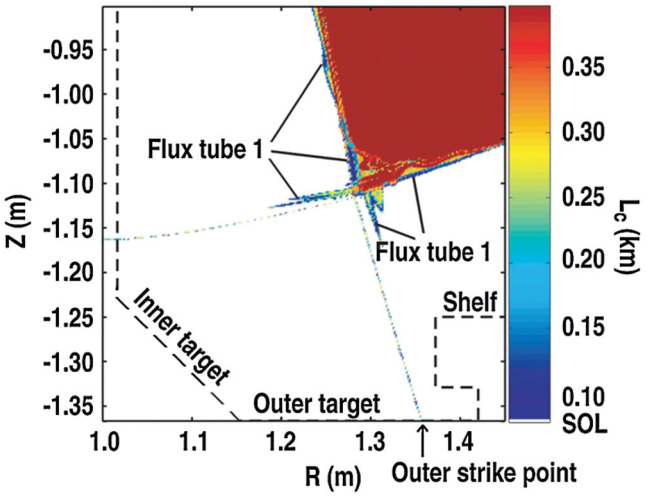

FIG. 1 (color). Connection length plot of the lower target area in DIII-D of shot no. 133908 at 2000 ms. The dashed line shows the wall of the vacuum vessel. The inner and outer targets are indicated as well as the shelf. The position of the outer strike point is marked by the black arrow.

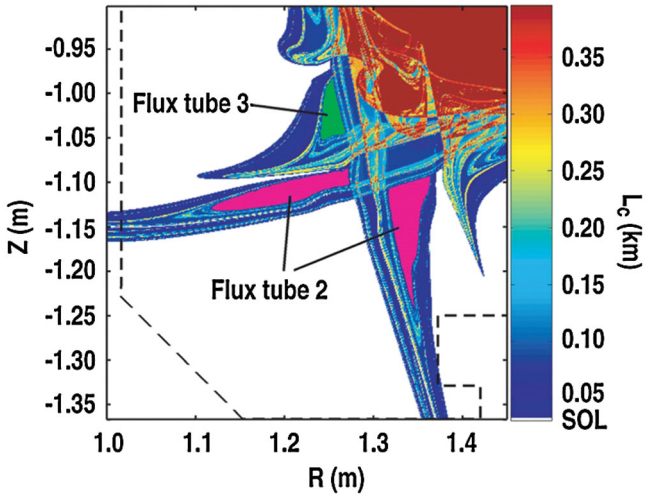

FIG. 2 (color). Poloidal cross section of the bifurcated structure produced when a 300 A current filament is driven in tube 1, shown in Fig. 1. Flux tube 2 is shown by the magenta areas and flux tube 3 by the green area. Their connection length is about 50 m. Note that the green and magenta colors are intended to highlight these flux tubes, and do not correspond to the color scale at the right.

SOL of the reference case. Therefore, the current in the tubes appears to be flowing on unperturbed SOL field lines in agreement with Ref. [14]. Here we pick the two largest tubes, marked in Fig. 2 as flux tube 2 (magenta) and flux tube 3 (green). Thereby, tube 3 is the 180° shifted counterpart of tube 2. Note that all one-poloidal-turn flux tubes have the same helical structure as either tube 2 or tube 3 and therefore produce similar $n = 2$ perturbations.

To estimate the current flowing through tubes 2 and 3 we assume the current density to be constant and scale the total current by the area of the flux tube. Current measurements are not available for all discharges. Therefore we adopt the value 150 A for the peak current flowing through the tiles from another discharge [16] with similar ELMs, to calibrate the current density. The calibration is based on the flux tube areas in the footprint, as shown in Fig. 3. Using the calibration, we can estimate the total current to be 4.6 kA. According to the individual areas of tubes 2 and 3 in the poloidal cross section, Fig. 2, we conclude that tube 2 carries a current of 2.8 kA and tube 3 carries a current of 1.8 kA. Using the same area scaling, we get a current of about 272 A in tube 1, which confirms our initial assumption and makes the present step scenario consistent.

Comparing with experiments we note that during shots in DIII-D a camera takes pictures of the shelf, located above the outer target, which starts at the major radius $R = 1.372$ m at $Z = -1.250$ m. During an ELM event stripes appear on the shelf, as can be seen in Fig. 4(a). The lowest, very bright stripe in the image is created by the outer strike point and marks the beginning of the shelf as well. Different tiles are clearly visible in the light of the discharge as well as an upward viewing vertical port located at $R = 1.486$ m, $\phi = 60°$ in the vessel near the right-hand edge of the of the shelf shown in Fig. 1. At the very

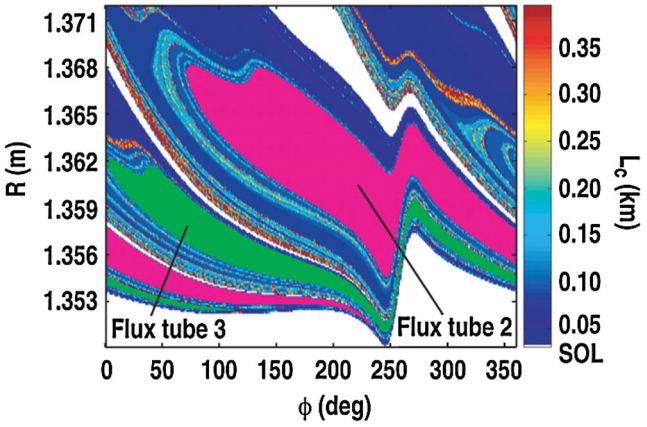

FIG. 3 (color). Connection length footprint on the outer target plate with the additional perturbation of the 300 A current filament in tube 1. Note that the outer target has a vertical step up to the shelf at $R = 1.372$ m (see Fig. 1), which is the top boundary of this figure. The toroidal angle is given in the left-handed machine related coordinate system. Flux tubes 2 and 3 are shown similar to Fig. 2.

beginning of the shelf a faint stripe is visible, which almost merges with the bright light from the strike point, located at $Z = -1.366$ m on the divertor target plate as seen in Fig. 1. Further out radially on the shelf three stripes are clearly visible, one right below the port, one very bright one hitting the lower part of the port, and a smaller one hitting the top of the port. These are typical stripe structures that appear on the shelf during ELMs; see also Ref. [5].

Figure 4(b) shows a connection length simulation of the same region on the shelf as in Fig. 4(a). The various tiles as well as the port are indicated by dashed lines. Note that the numerical predictions are depicted in cylindrical coordinates while the camera observations in Fig. 4(a) are shown in Cartesian coordinates. The different projection explains the missing curvature in Fig. 4(b). The numerical model, which includes the thermoelectric currents in the flux tubes, clearly shows nearly the same ELM stripe structure as in the camera image. There are small stripes at the very edge of the shelf, which is the bottom boundary in the figure. A large stripe with high connection length hits the lower part of the port and a small stripe hits the upper part. The major radius of the stripes increases with decreasing toroidal angle. The same trend is clearly visible in the camera image. So, by taking into account the thermoelectric currents in short connection length flux tubes, ELM stripe structures can be reproduced numerically with good accuracy.

The model presented here has certain limitations. First, it is not completely self-consistent since an iterative two-step description was used. Therefore, it is not practical to determine the time scale of the ELM. For simplicity only the two largest flux tubes were used for conducting current, producing a $n = 2$ perturbation. Of course, many more flux tubes are present. Running current through all available flux tubes could create a perturbation with higher n numbers as measured in DIII-D [18]. Also, only single current filaments were used here instead of a more realistic current distribution over the whole flux tube area.

Despite these limitations, in this Letter it is shown that typical ELM stripe structures can be correctly modeled when thermoelectric currents and the corresponding change of magnetic topology are incorporated. The stripes in the connection length plot, Fig. 4(b), appear at the same positions, radially and toroidally, and with the same radial outward trend as in the camera observation in the discharge. The currents used in the model are scaled in agreement with current measurements during ELM events. Furthermore, the simulation shows, indirectly through the formation of the new flux tubes, that a connection of the plasma with the upper targets is established during the process. The simulations presented here confirm the scenario proposed in Ref. [16]. This Letter advances the ELM modeling by showing that the change in magnetic topology due to thermoelectric currents leads to a self-amplification

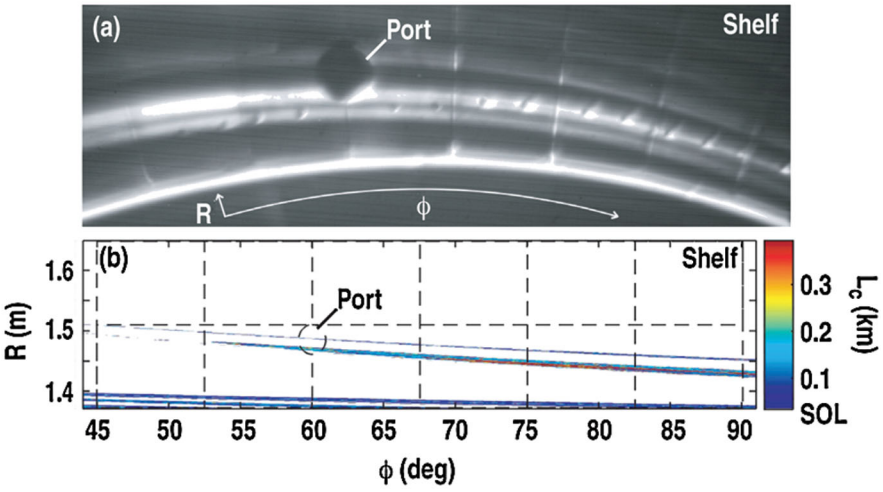

FIG. 4 (color). (a) Infrared camera observation of an ELM event. Shot no. 133908 close to 2000 ms. The camera view shows the shelf, starting at $R = 1.372$ m and $Z = -1.250$ m (below the equatorial plane of the tokamak), around the port at $\phi = 60°$, visible as a dark circle. As seen in Fig. 1, the outer target plate is located at $Z = -1.366$ m or 0.116 m below the top of the shelf. (b) Connection length plot of the same section on the shelf as shown in (a). The dashed lines indicate the different tiles and the port, as they are visible in the camera picture. Currents of 300 A in tube 1, 2.8 kA in tube 2, and 1.8 kA in tube 3 are used in the numerical model to produce the striped footprint pattern on the top of the shelf.

as proposed by Ref. [15] as well as a current distribution similar to the SOL currents in Ref. [14]. But a natural limitation of the currents due to position and size of the flux tubes is introduced. Furthermore, it has been shown that the seed flux tubes needed to initiate this process are generated by small nonaxisymmetric magnetic perturbations such as field errors which are always present in magnetic confinement devices like tokamaks. Although only a single fixed error field and equilibrium was used in this Letter, the simulated stripe patterns are sensitive to fluctuations in the reference case topology. A more detailed study of the sensitivity will be done in the future. Fluctuating error fields provide a mechanism for variations in the ELM-to-ELM footprint pattern.

In future work further validation against the experiment is planned together with improving the model with respect to the limitations mentioned above. In particular, the effect of a broader current distribution within the flux tubes and more filaments will be investigated. Preliminary results show already that the main features of the simulation discussed here remain valid while an even more complex substructure may be created. The effect of other types of RMPs on the ELM structures will be studied in the future with the main goal to predict and understand ELM suppression numerically.

Discussions with R. A. Moyer, O. Schmitz, and M. Jakubowski are gratefully acknowledged. This work was supported by the U.S. Department of Energy under DE-FC02-04ER54698, DE-AC52-07NA27344, and DE-FG02-05ER54809, as well as the DFG under project SP229/1-1.

[1] H. Zohm, Plasma Phys. Controlled Fusion **38**, 1213 (1996).
[2] M. Shimada *et al.*, Nucl. Fusion **47**, S1 (2007).
[3] A. Loarte *et al.*, Plasma Phys. Controlled Fusion **45**, 1549 (2003).
[4] H. R. Wilson *et al.*, Plasma Phys. Controlled Fusion **48**, A71 (2006).
[5] T. Eich *et al.*, Phys. Rev. Lett. **91**, 195003 (2003).
[6] A. Kirk *et al.*, Phys. Rev. Lett. **96**, 185001 (2006).
[7] T. E. Evans *et al.*, Nature Phys. **2**, 419 (2006).
[8] T. E. Evans *et al.*, Phys. Rev. Lett. **92**, 235003 (2004).
[9] Y. Liang *et al.*, Phys. Rev. Lett. **98**, 265004 (2007).
[10] M. Becoulét *et al.*, Nucl. Fusion **48**, 024003 (2008).
[11] M. J. Schaffer *et al.*, Nucl. Fusion **48**, 024004 (2008).
[12] A. Wingen *et al.*, Phys. Plasmas **16**, 042504 (2009).
[13] A. Wingen *et al.*, Nucl. Fusion **49**, 055027 (2009).
[14] H. Takahashi *et al.*, Phys. Rev. Lett. **100**, 205001 (2008).
[15] L. J. Zheng *et al.*, Phys. Rev. Lett. **100**, 115001 (2008).
[16] T. E. Evans *et al.*, J. Nucl. Mater. **390–391**, 789 (2009).
[17] G. M. Staebler and F. L. Hinton, Nucl. Fusion **29**, 1820 (1989).
[18] J. H. Yu *et al.*, Phys. Plasmas **15**, 032504 (2008).